ORIGINAL ARTICLE

lajss.org© Latin American Journal of Solids and Structures

www.lajss.org

# Nonlinear Dynamic Response and Stability Analysis of a Tensegrity Bridge to Selected Cable Rupture

**Nabil Ben Kahla[a,b]* Mohamed Hechmi El Ouni[a,b,c] Nizar Bel Hadj Ali[b] Roohul Abad Khan[a]**

[a] Department of Civil Engineering, College of Engineering, King Khalid University, Abha, Kingdom of Saudi Arabia.
Email: nbohlal@kku.edu.sa, melouni@kku.edu.sa, rakhan@kku.edu.sa
[b] Laboratory of Systems and Applied Mechanics, Tunisia Polytechnic School, University of Carthage, La Marsa, Tunis, Tunisia.
Email: nizar.belhadjali@gmail.com
[c] Higher Institute of Applied Sciences and Technologies of Sousse, University of Sousse, Sousse, Tunisia.

* Corresponding author

http://dx.doi.org/10.1590/1679-78255907

**Abstract**

This paper presents a nonlinear dynamic analysis procedure used for the investigation of the response of a tensegrity bridge to a selected sudden cable rupture. In order to simulate a cable rupture, for the loaded or unloaded geometry of the tensegrity structure, a geometrical nonlinear analysis is performed, and the cable end tensions projected in the global coordinate system are determined. Next, these forces are applied as external nodal forces to the tensegrity structure, from which the selected cable has been omitted (damaged structure). Next, the nonlinear equation of motion of the tensegrity bridge subjected to dynamic loads is discretized and integrated in time using the unconditionally stable Newmark constant-average acceleration method combined with a Newton-Raphson iterative scheme. The dynamic simulation is initiated by cancelling the vector of external forces representing the damaged cable. For each case, the largest tension force in the cables, the largest compression force in the struts as well as the largest average midspan displacement are determined. The maximum tension obtained in all the bridge cables was way below their tension capacities for the unloaded bridge and exceeded them for only one case of the loaded one. However, the maximum compression forces obtained in the struts of the bridge were below their compression capacities. The limit deflection has been exceeded only for of the loaded bridge and for several cases of cable rupture. Nonlinear dynamic instabilities caused by cable slackening were observed in all simulations.

**Keywords:**

Tensegrity Bridge; Dynamic stability; cable rupture;

Received: December 19, 2019. In revised form: February 08, 2020. Accepted: February 10, 2020. Available online: February 12, 2020.
https://doi.org/10.1590/1679-78255907

**Graphical Abstract**

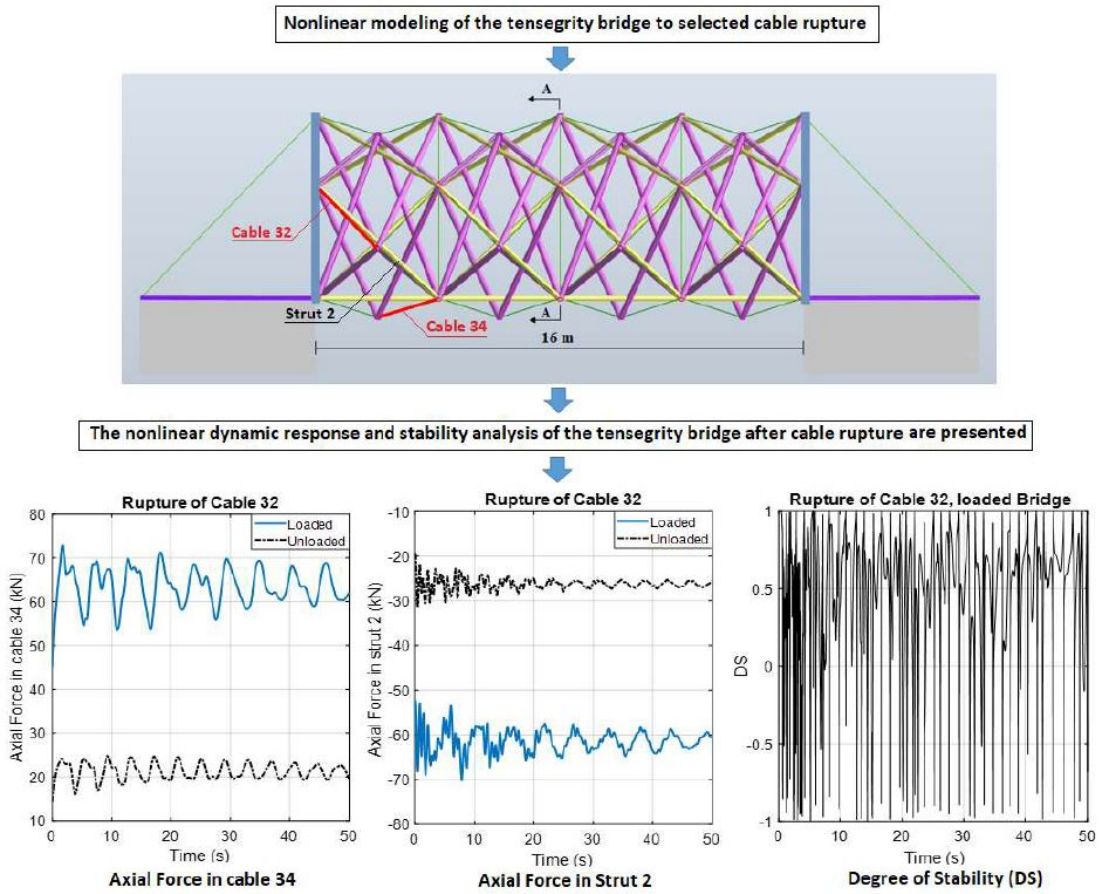


## 1 INTRODUCTION

"Tensegrity" systems are lightweight spatial reticulated structures combining cables in tension and bars in compression in a self-equilibrated state providing stiffness and stability to the system. The word tensegrity, proposed by Fuller in 1962, comes from the elision of tensile and integrity. The concept of tensegrity was born in the field of art (architecture and sculpture), and then inspired generations of researchers in various disciplines, especially in civil engineering, aerospace, marine engineering and biomedical (Skelton and de Oliveira, 2009). Tensegrity systems have in general high strength-to-mass ratio and low structural damping which make them sensitive to vibrations induced by traffic, wind and earthquakes. Such loads could affect their serviceability and user's comfort and even cause structural damage or failure.

Tensegrity systems are in general both kinematically and statically indeterminate and they exhibit large displacements which makes modeling their nonlinear dynamic a challenging task. This have attracted many researchers in the past 20 years. Motro et al. (1986) pioneered the investigations of the dynamics of tensgerity structures and proposed a linearized dynamic model around an equilibrium configuration to study the nonlinear behavior of a simple tensegrity structure composed of nine cables and three struts. Kebiche et al. (1999) performed a geometrical nonlinear elastic analysis of tensegrity systems using the total Lagrangian formulation. Ben Kahla and Kebiche (2000) investigated the nonlinear elasto-plastic behavior of a tensegrity beam system made of five quadruplex module assembled together, using an updated Lagrangian formulation. Later, Ben Kahla and Moussa (2002) analyzed the effect of a cable rupture on simple tensegrity systems.

Oppenheim and Williams (2001) investigated the dynamic behavior of a simple tensegrity structure and showed that the tensegrity elements natural damping is affected by the presence of mechanisms which are infinitesimal in nature. Sultan et al. (2002) proposed a linearized dynamic model for two classes of tensegrity

systems and proved that systems pretensions directly affect their modal dynamic range. Tan and Pellegrino (2008) analyzed the nonlinear dynamic behavior of a cable-stiffened pantographic deployable structure. They proved that the frequencies depend on the pretension level of the active cables. Bel Hadj Ali and Smith (2010) exploited this property to perform vibration control of a five-module tensegrity structure. Bel Hadj Ali et al. (2010) studied the static and dynamic behavior of a tensegrity-based pedestrian bridge and showed that such type of structure could be a viable solution for small span footbridges.

Based on both total and updated Lagrangian formulations, Tran and Lee (2011) developed a model for tensegrity systems accounting for both geometric and material nonlinearities. Faroughi and Lee (2014) proposed a geometric nonlinear model using a co-rotational technique. Vibrations may cause instability of tensegrity systems or even partial of total collapse of the structure. In the literature, only few papers have investigated the dynamic stability of tensegrity systems. Stability of tensegrity frameworks was investigated by Connelly and Terrell (2005) for some prismatic systems. The global instability of a simple tensegrity system and the local-Euler-buckling of the bars were studied by Lazopoulos (2005), who investigated the critical conditions and the post-critical behavior. Based on the eigenvectors and eigenvalues properties of the geometrical stiffness matrices, Ohsaki and Zhang (2006) derived the stability conditions of tensegrity structures. Michielsen et al. (2012) proposed two criterions to assess upper bounds for the harmonic excitation amplitude and prevent the dynamic instability of tensegrity systems.

Although nonlinear dynamic analysis is intensively investigated by researchers, most of existing studies were conducted on simple tensegrity systems. With the appearance of complex spatial tensegrity structures such us domes and bridges, the investigations of nonlinear behavior and stability of these structures become a new challenge. Xiao et al. (2011) examined the active vibration control of a tensegrity dome of Levy type subjected to wind excitation using an instantaneous optimal control algorithm. El Ouni and Ben Kahla (2014) investigated the control of a Geiger tensegrity dome using active tendon employing decentralized collocated Integral Force Feedback. Sychterz and Smith (2018) proposed an interesting method to detect and locate ruptured cables on a deployable tensegrity footbridge based on experimental vibration measurements. Al Sabouni-Zawadzka and Gilewski (2018) discussed the inherit properties of smart tensegrity systems including self-control, self-diagnosis, self-repair and self-adjustment. Recently, Atig et al. (2019) studied the dynamic stability of a Geiger's dome and focused on the effect of active damping on the stability of the structure. González et al (2019) proposed a new reconfiguration strategy for actuated multistage tensegrity structuresusing infinitesimal mechanism. They combined the force density method with a marching procedure to solve the equilibrium problem based on differential equations defining the kinematic constraints of the system. Oh et al (2019) presented an incremental analysis procedure for shape change of tensegrities through forced elongation of cables.

Although, the tensegrity concept is increasingly adopted in built structural systems, many engineers still have queries about this type of structures especially in relation with their nonlinear behavior and stability under cable rupture. This has inspired the authors to perform a nonlinear dynamic and stability analysis of a 16m pedestrian tensegrity bridge under cable rupture. The nonlinear equation of motion of the tensegrity bridge subjected to dynamic loads is discretized and integrated in time using the unconditionally stable Newmark constant-average acceleration method combined with a Newton-Raphson iterative scheme. The proposed stability criterion is a time-varying degree of stability based on the variation in strain energy and its complementary part. The effect of the cable rupture on the displacements of critical points and member internal forces as well as on the stability criterion are discussed.

## 2 STRUCTURAL MODELLING

In order to correctly model the nonlinear behavior of a tensegrity structure, a nonlinear space truss idealization is used for both cables and struts (Blandford, 1996; Leu and Yang, 1990). According to this formulation, the local stiffness matrix of a space truss element (*ij*), defined by its end nodes *i* and *j* and whose nodal displacement vectors in the local element coordinate system (*x, y, z*) (*x* being along the element axis) respectively at node *i* and *j* are $[u_i, v_i, w_i]^T$ and $[u_j, v_j, w_j]^T$; is given by

$$[k] = [k_e] + [k_g] + [k_{nl}] \tag{1}$$

In which the element local elastic stiffness matrix is $[k_e]$, the element local geometric stiffness matrix is $[k_g]$ and $[k_{nl}]$ is the local nonlinear element stiffness matrix. Let *A*, *E*, *L* and *F* be respectively the element cross-section area, the element material modulus of elasticity, the element length and the element axial force, then the element local elastic stiffness matrix $[k_e]$ is expressed as

$$[k_e] = \begin{bmatrix} S_e & -S_e \\ -S_e & S_e \end{bmatrix} \tag{2}$$

$[S_e]$is a 3×3 matrix whose elements are null but the following ones

$$(S_e)_{11} = (S_e)_{44} = -(S_e)_{14} = -(S_e)_{41} = \frac{AE}{L} \tag{3}$$

the element local geometric stiffness matrix$[k_g]$is written as follows

$$[k_g] = \begin{bmatrix} S_g & -S_g \\ -S_g & S_g \end{bmatrix} \tag{4}$$

Where $[S_g]$is a 3×3 diagonal matrix whose elements are zeros but the ones given hereafter

$$(S_g)_{11} = (S)_{22} = (S_g)_{33} = \frac{F}{L} \tag{5}$$

and the local nonlinear element stiffness matrix is given by

$$[k_{nl}] = \begin{bmatrix} S_{nl} & -S_{nl} \\ -S_{nl} & S_{nl} \end{bmatrix} \tag{6}$$

In which$[S_{nl}]$is a 3×3 matrix whose elements are defined as follows, by letting$\Delta u = u_j\text{-}u_i$, $\Delta v = v_j\text{-}v_i$ and $\Delta w = w_j\text{-}w_i$, then it comes that

$$(S_{nl})_{11} = \frac{AE}{L^2}\left[3\Delta u + \frac{1}{2L}(3\Delta u^2 + \Delta v^2 + \Delta w^2)\right] \tag{7}$$

$$(S_{nl})_{22} = \frac{AE}{L^2}\left[\Delta u + \frac{1}{2L}(\Delta u^2 + 3\Delta v^2 + \Delta w^2)\right] \tag{8}$$

$$(S_{nl})_{33} = \frac{AE}{L^2}\left[\Delta u + \frac{1}{2L}(\Delta u^2 + \Delta v^2 + 3\Delta w^2)\right] \tag{9}$$

$$(S_{nl})_{21} = (S_{nl})_{12} = \frac{AE}{L^2}\left[\Delta v + \frac{1}{L}(\Delta u \Delta v)\right] \tag{10}$$

$$(S_{nl})_{31} = (S_{nl})_{13} = \frac{AE}{L^2}\left[\Delta w + \frac{1}{L}(\Delta u \Delta v)\right] \tag{11}$$

$$(S_{nl})_{32} = (S_{nl})_{23} = \frac{AE}{L^2}\left[\frac{1}{L}(\Delta v \Delta w)\right] \tag{12}$$

## 3 NONLINEAR STATIC ANALYSIS

The incremental stiffness equation expressing the geometric nonlinear equilibrium of a tensegrity structure is given by

$$[K]^p\{X\}^p = \{F\}^p \tag{13}$$

In which: $[K]$is the structure stiffness matrix, $\{X\}$ the vector of displacements and $\{F\}$ is the vector of nodal applied forces and *p* is the iteration number.

$$\{F\}^p = \{F^{ext}\} - \{F_B\}^p \tag{14}$$

Where$\{F_B\}$ is the vector of unbalanced forces and $\{F^{ext}\}$ is the vector of nodal external forces.

In order to simulate a broken cable, for the loaded or unloaded geometry of the tensegrity structure, a geometrical nonlinear analysis is performed, and the cable end tensions projected in the global coordinate system are determined. Next, these forces are applied as external nodal forces to the tensegrity structure, from which the selected cable has been omitted (damaged structure), and a second geometrical nonlinear analysis is undertaken to check the correctness of the procedure, i.e. to verify that the same internal forces are obtained as for the intact structure. For this second analysis, the stiffness equation becomes:

$$[K_d]^p\{X\}^p = \{F^{ext}\} - \{F_{Cint}\} - \{F_B\}^p \tag{15}$$

With $[K_d]$ being the damaged tensegrity structure stiffness matrix, $\{F_{Cint}\}$ is a vector whose elements are all equal zeros but the lines corresponding to the degrees of freedom associated with the nodes at the extremities of the broken cables, which will contain the values of the projected cable end tension.

## 4NONLINEAR DYNAMIC ANALYSIS

The nonlinear equation of motion of a tensegrity structure subjected to dynamic loading is expressed at time *t* as follows:

$$[M]\{\ddot{X}\} + [C]\{\dot{X}\} + [K]\{X\} = \{F\} \tag{16}$$

$[M]$is the structure mass matrix, $[C]$ is the structure damping matrix and $[K]$ is the structure stiffness matrix. $\{\ddot{X}\}$, $\{\dot{X}\}$and $\{X\}$are respectively the vectors of the nodal accelerations, velocities and displacements, whereas $\{F\}$ is the vector of the nodal applied forces.

The equation of motion discretized at the instant $t + \Delta t$, where $\Delta t$ is the time increment, can be expressed as follows

$$[M]\{\ddot{X}\}_{t+\Delta t} + [C]\{\dot{X}\}_{t+\Delta t} + [K]_{t+\Delta t}\{X\}_{t+\Delta t} = \{\Delta F\}_{t+\Delta t} \tag{17}$$

Which can be written as

$$[M]\{\ddot{X}\}_{t+\Delta t} + [C]\{\dot{X}\}_{t+\Delta t} + [K]_{t+\Delta t}\{X\}_{t+\Delta t} = \{F^{ext}\}_{t+\Delta t} - \{F_B\}_{t+\Delta t} \tag{18}$$

With

$$\{\Delta F\}_{t+\Delta t} = \{F^{ext}\}_{t+\Delta t} - \{F_B\}_{t+\Delta t} \tag{19}$$

Equation (19) is written as

$$\{F_B\}_{t+\Delta t} = \{F^{ext}\}_{t+\Delta t} - [M]\{\ddot{X}\}_{t+\Delta t} - [C]\{\dot{X}\}_{t+\Delta t} - [K]_{t+\Delta t}\{X\}_{t+\Delta t} \tag{20}$$

using an updated Lagrangian formulation, the incremental form of Equation (18) is

$$\{F_B\}_{t+\Delta t} = \{F^{ext}\}_{t+\Delta t} - [M]\{\Delta\ddot{X}\}_{t+\Delta t} - [C]\{\Delta\dot{X}\}_{t+\Delta t} - [K]_{t+\Delta t}\{\Delta X\}_{t+\Delta t} \tag{21}$$

The unconditionally stable Newmark constant-average acceleration method is used to integrate Eqn. 21 in time. The incremental acceleration and velocity vectors are expressed as follows:

$$\{\Delta\ddot{X}\}_{t+\Delta t} = \frac{4}{\Delta t^2}\{\Delta X\}_{t+\Delta t} - \frac{4}{\Delta t}\{\dot{X}\}_t - \{\ddot{X}\}_t \tag{22}$$

$$\{\Delta\dot{X}\}_{t+\Delta t} = \frac{2}{\Delta t}\{\Delta X\}_{t+\Delta t} - \{\dot{X}\}_t \tag{23}$$

With

$$\{\Delta\dot{X}\}_{t+\Delta t} = \frac{2}{\Delta t}\{\Delta X\}_{t+\Delta t} - \{\dot{X}\}_t \quad (24)$$

Combining Eqns. 22 and 23 with Eqn. 21and introducing the effective stiffness matrix and the effective incremental load vector, yields

$$[\widetilde{K}]_{t+\Delta t}\{\Delta X\}_{t+\Delta t} = \{\Delta\widetilde{F}\}_{t+\Delta t} \quad (25)$$

With

$$[\widetilde{K}]_{t+\Delta t} = \frac{4}{\Delta t^2}[M] + \frac{2}{\Delta t}[C] + [K]_{t+\Delta t} \quad (26)$$

and

$$\{\Delta\widetilde{F}\}_{t+\Delta t} = \{\Delta F\}_{t+\Delta t} + [M]\left(\frac{4}{\Delta t^2}\{X\}_t + \frac{4}{\Delta t}\{\dot{X}\}_t + \{\ddot{X}\}_t\right) + [C]\left(\frac{2}{\Delta t}\{X\}_t + \{\dot{X}\}_t\right) \quad (27)$$

An iterative scheme based on a modified Newton-Raphson method is used to balance residual forces within each time step. At iteration p, Equation (25) is written as:

$$[\widetilde{K}]^p_{t+\Delta t}\{\Delta X\}^p_{t+\Delta t} = \{\Delta\widetilde{F}\}^p_{t+\Delta t} \quad (28)$$

In which the error estimate is

$$\{\Delta X\}^p_{t+\Delta t} = \{X\}^p_{t+\Delta t} - \{X\}_t \quad (29)$$

Thus

$$\{X\}^p_{t+\Delta t} = \{X\}_t + \{\Delta X\}^p_{t+\Delta t} \quad (30)$$

The effective stiffness matrix and the effective incremental load vector at iteration p are expressed respectively as:

$$[\widetilde{K}]^p_{t+\Delta t} = \frac{4}{\Delta t^2}[M] + \frac{2}{\Delta t}[C] + [K]^p_{t+\Delta t} \quad (31)$$

And

$$\{\Delta\widetilde{F}\}^p_{t+\Delta t} = \{\Delta F\}^p_{t+\Delta t} + [M]\left(\frac{4}{\Delta t^2}\{X\}_t + \frac{4}{\Delta t}\{\dot{X}\}_t + \{\ddot{X}\}_t\right) + [C]\left(\frac{2}{\Delta t}\{X\}_t + \{\dot{X}\}_t\right) \quad (32)$$

With

$$\{\Delta F\}^p_{t+\Delta t} = \{F^{ext}\}_{t+\Delta t} - \{F_B\}^p_{t+\Delta t} \quad (33)$$

And

$$\{F_B\}^p_{t+\Delta t} = \{F^{ext}\}_{t+\Delta t} - [M]\{\Delta\ddot{X}\}^p_{t+\Delta t} - [C]\{\Delta\dot{X}\}^p_{t+\Delta t} - [K]^p_{t+\Delta t}\{\Delta X\}^p_{t+\Delta t} \quad (34)$$

The iterative procedure described above is repeated until the following convergence criterion is satisfied:

$$\left\| \frac{\{X\}_{t+\Delta t}^{p+1} - \{X\}_{t+\Delta t}^{p}}{\{X\}_{t+\Delta t}^{p}} \right\| \leq \varepsilon \tag{35}$$

The described numerical scheme can be used for the dynamic analysis of a tensegrity structure under any dynamic loading. For the current study, the objective is to investigate the dynamic behavior and the stability of a tensegrity structure after a unique cable rupture. For this, the cable rupture is simulated by cancelling the vector of external forces representing the damaged cable and tracing the damped dynamic behavior of the structure until it rests in an equilibrium position.

## 5 DYNAMIC STABILITY

The variations in strain energy and its complementary part at time *t+Δt* can be described by Equations (36) and (37), respectively. Notice that the incremental form is used in these two equations.

$$\{\Delta U\}_{t+\Delta t}^{p} = \left\{\{X\}_{t+\Delta t}^{p}\right\}^{T} [K_c]_{t+\Delta t} \{\Delta X\}_{t+\Delta t}^{p} + \frac{1}{2} \left\{\{\Delta X\}_{t+\Delta t}^{p}\right\}^{T} [K]_{t+\Delta t}^{p} \{\Delta X\}_{t+\Delta t}^{p} \tag{36}$$

$$\{\Delta U^{*}\}_{t+\Delta t}^{p} = \left\{\{X\}_{t+\Delta t}^{p}\right\}^{T} [K]_{t+\Delta t}^{p} \{\Delta X\}_{t+\Delta t}^{p} + \frac{1}{2} \left\{\{\Delta X\}_{t+\Delta t}^{p}\right\}^{T} [K]_{t+\Delta t}^{p} \{\Delta X\}_{t+\Delta t}^{p} \tag{37}$$

$[K_c]$is the secant stiffness matrix which is evaluated only once at the beginning of the iteration. An expression relating the variations in strain energy to the variation in the complementary strain energy can be obtained by combining equations (36) and (37),

$$\{\Delta U\}_{t+\Delta t}^{p} = \left( \frac{\left\{\{X\}_{t+\Delta t}^{p}\right\}^{T} [K_c]_{t+\Delta t} \{\Delta X\}_{t+\Delta t}^{p} + \frac{1}{2} \left\{\{\Delta X\}_{t+\Delta t}^{p}\right\}^{T} [K]_{t+\Delta t}^{p} \{\Delta X\}_{t+\Delta t}^{p}}{\left\{\{X\}_{t+\Delta t}^{p}\right\}^{T} [K]_{t+\Delta t}^{p} \{\Delta X\}_{t+\Delta t}^{p} + \frac{1}{2} \left\{\{\Delta X\}_{t+\Delta t}^{p}\right\}^{T} [K]_{t+\Delta t}^{p} \{\Delta X\}_{t+\Delta t}^{p}} \right) \{\Delta U^{*}\}_{t+\Delta t}^{p} \tag{38}$$

If this equation is plotted, taking for abscissa axis $\Delta U$ and for the ordinate one $\Delta U^{*}$, then a straight line appears and crosses the origin. The slope is given by

$$tan\left(\theta_{t+\Delta t}^{p}\right) = \frac{\left\{\{X\}_{t+\Delta t}^{p}\right\}^{T} [K_c]_{t+\Delta t} \{\Delta X\}_{t+\Delta t}^{p} + \frac{1}{2} \left\{\{\Delta X\}_{t+\Delta t}^{p}\right\}^{T} [K]_{t+\Delta t}^{p} \{\Delta X\}_{t+\Delta t}^{p}}{\left\{\{X\}_{t+\Delta t}^{p}\right\}^{T} [K]_{t+\Delta t}^{p} \{\Delta X\}_{t+\Delta t}^{p} + \frac{1}{2} \left\{\{\Delta X\}_{t+\Delta t}^{p}\right\}^{T} [K]_{t+\Delta t}^{p} \{\Delta X\}_{t+\Delta t}^{p}} \tag{39}$$

For stable linear elastic systems, $\theta$is constant and equal to $\pi/4$. When $\theta$ lies in the intervals [0, $\pi/2$] and [$\pi$, $3\pi/2$], it corresponds to nonlinear stable structures. Else for systems displayinginstabilities, $\theta$ belongs to the intervals [$\pi/2$, $\pi$] and [$3\pi/2$, $2\pi$]. This metric can thus be used to check the possible instabilities experienced by the structure after damage (He et al., 2003).

$$(DSF)_{t+\Delta t}^{p} = 1 - \left| \frac{\theta_{t+\Delta t}^{p}}{\left(\frac{\pi}{4}\right)} - 1 \right| \tag{40}$$

If DSF(t) is positive, the system is stable; else, when DSF(t) is negative, the system is considered unstable.

## 6 DESCRIPTION OF THE TENSEGRITY BRIDGE

The studied structure is a tensegrity bridge spanning 16 m, shown in Figure 1. It is made up of four pentagon modules, each one spans 4 m with an inner radius of 3.12 m. The bridge is composed of 45 nodes, 60 struts and 105 cables. Struts are classified into “diagonal” and “intermediate” struts and cables are categorized into “layer cables” and “X-cables” depending on their geometric position. All cable elements are assumed to be discontinuous and firmly attached to the structure nodes. Thus, the nodes of the outer and inner pentagon are linked by diagonal struts, those of the middle pentagon are linked to outer and inner pentagon nodes by the intermediate struts. As for the middle pentagon nodes, they are linked to those of the inner and outer pentagon by X-cables. Finally, the nodes of the two outer pentagons are linked by Layer cables

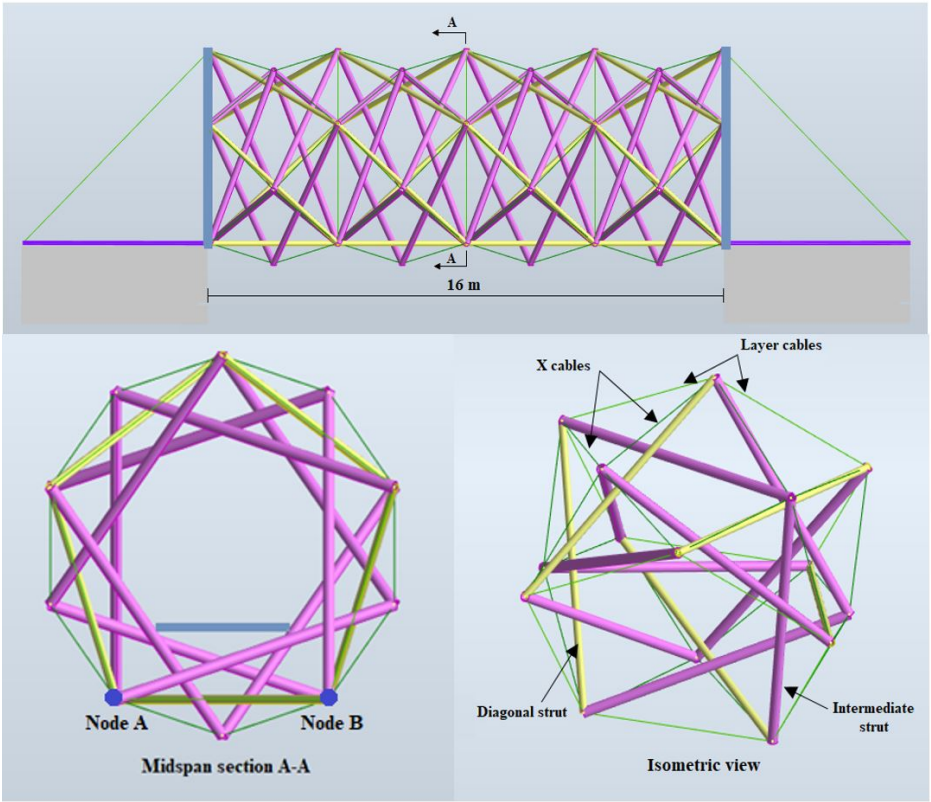


**Figure 1.** Side view of the tensegrity bridge and the basic pentagonal module

Intermediate and diagonal struts are hollow-tube profiles and have the same length of 5.42 m. The lengths of X-cables and layer cables are 2.77 m and 3.66 m respectively. The density of steel elements is equal to 78.5 KN/m$^3$. The Young's modulus of the struts and cables are equal to 210 GPa and 115 GPa respectively. The self-stress and geometric properties of the elements are given in Table 1.

**Table 1.** Properties of the tensegrity bridge elements.

| *Member* | *Diameter (mm)* | *Cross-sectional area (mm$^2$)* | *Self-stress ratio (%)* | *Tension/Compression Capacity(kN)* |
|---|---|---|---|---|
| struts | 89 | 1320 | - | 71.05 |
| Layer cables | 9 | 63.6 | 22.5 | 67.92 |
| X-Cables | 9 | 63.6 | 22.5 | 67.92 |

The motion of extremity nodes (supports) are restrained in all directions (X, Y and Z). Hence, the total number of degrees of freedom is equal to 105, each inner node has three degrees of freedom in the order X, Y then Z. The tensegrity bridge has 60 independent self-stress states and no internal mechanism. It is statically indeterminate and kinetically determinate structure. In order for the structure to be in equilibrium, an initial pre-stressing of the structure is needed. A general state of self-stress would be any linear combination of the 60 independent self-stress states. Thus a 22.5% of the tension capacity of the cable element tension capacity were used to pre-tension all the cables of the tensegrity bridge. Hence, all the cables were pre-stress with a tension equal to 15.282kN. Next, a nonlinear geometric static analysis of the structure subjected to only the pre-stress was performed to determine the initial forces in the elements making up the tensegrity bridge in its initial equilibrium configuration, the results are shown in Table 2. the results are given for the elements of the first two modules. For those of the third and fourth module, they are deduced

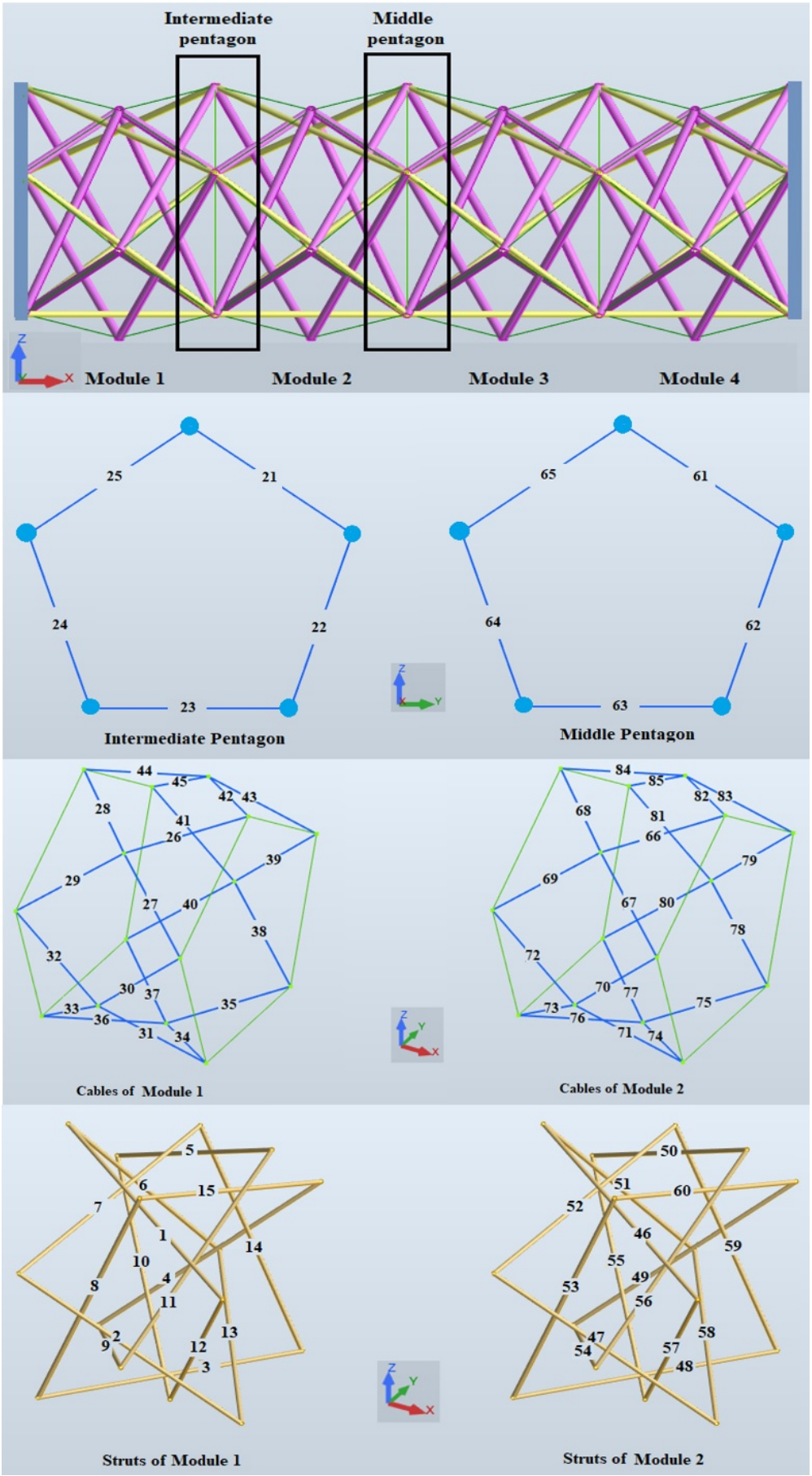


**Figure 2.** Numbering of cablesand strutsof the two first modules of the tensegrity bridge.

by symmetry. A natural damping of 1% is assumed for all modes of the structure. Figure 2 displays the numbering of cable elements of the two first modules of the tensegrity bridge. Exploiting the symmetry of the structure, cable rupture was simulated for all layer and X-cables belonging to first and second pentagonal modules.

**Table 2.** Initial forces in the elements of the left half of the tensegrity bridge.

| *Modules* | *Group of elements* | *Elements* | *Initial forces (KN)* |
|---|---|---|---|
| 1 | Diagonal struts | 1, 2, 3, 4, 5 | -19.516 |
| | Intermediate struts | 6, 7, 8, 9, 10 | -7.5689 |
| | | 11, 12, 13, 14, 15 | -9.5791 |
| | Layer cables | 21, 22, 23, 24, 25 | 13.8212 |
| | X-cables | 26, 30, 34, 38, 43 | 15.1380 |
| | | 27, 31, 35, 39, 42 | 14.4134 |
| | | 28, 32, 36, 40, 45 | 15.7561 |
| | | 29, 33, 37, 41, 44 | 14.8205 |
| 2 | Diagonal struts | 46, 47, 48, 49, 50 | -19.9251 |
| | Intermediate struts | 51, 52, 53, 54, 55 | -8.5938 |
| | | 56, 57, 58, 59, 60 | -8.8535 |
| | Layer cables | 61, 62, 63, 64, 65 | 13.6323 |
| | X-cables | 66, 70, 74, 78, 83 | 15.3534 |
| | | 67, 71, 75, 79, 82 | 15.1405 |
| | | 68, 72, 76, 80, 85 | 15.3140 |
| | | 69, 73, 77, 81, 84 | 15.3123 |

## 7 NUMERICAL SIMULATIONS

Two cases of the tensegrity bridge were considered. First the bridge was considered unloaded, then it was loaded at lower nodes of the intermediate and middle pentagons (nodes A and B in Figure 1). Thus, six vertical downward forces of magnitude 36.75 kN were applied at these six nodes. These loads are intended to simulate the service situation of the bridge.

For each case, 50 simulations of sudden cable rupture (member loss) were performed. 5 simulations for the sudden rupture of each layer cable of the intermediate pentagon and 5 simulations for the sudden rupture of each layer cable of the middle pentagon, plus 20 simulations for the sudden rupture of each x-cable of the first module and 20 simulations for the sudden rupture of each x-cable of the second module. For each simulation, a nonlinear dynamic analysis of the tensegrity bridge for a given cable loss is performed as mentioned above. For each case, the largest tension force in the cables, the largest compression force in the struts as well as the largest average midspan displacement of nodes A and B are obtained and plotted for each group of cable rupture simulations (Fig. 3 to Fig. 11). Figure 3 shows that in the case of the rupture of one element belonging to the x-cables of the first pentagon, the maximum tension obtained in all the bridge cables was way below their tension capacities for the unloaded bridge case. As for loaded bridge case, important values were obtained for the maximum tension in all the bridge cables but were below their tension capacities, only for the rupture of cable 32, the maximum tension has exceeded the cable tension capacity, which was obtained for cable 34. As for the case of the rupture of one element belonging to the x-cables of the second pentagon, the maximum tension obtained in all the bridge cables did not exceed their tension capacities for the unloaded and loaded bridge cases, which is displayed in Figure 4. Figures 5 and 6 show the maximum compression force obtained in the struts of the bridge for all x-cable rupture simulations and for the two load cases. These figures reveal that the maximum axial forces in the struts remained below their compression capacities in all cases. The Maximum average midspan vertical displacement of nodes A and B are plotted in Figure 7 and Figure 8 for the simulation of the rupture of x-cables in the first and the second pentagonal module and for the two load case considered. Results show that when the structure is unloaded, the maximum vertical average midspan displacement did not exceed the allowable deflection estimated at 2.2cm (span length/700), i.e the maximum displacement of the two midspan nodes (A and B) under Servicibility Limit State. As a matter of fact, the largest value obtained was 0.75 cm, and it was obtained for the rupture of the x-cable of the second pentagon numbered 80 as seen in Figure 8. However, in the case of the loaded bridge, the limit deflection has been exceeded in several cases of the rupture of the x-cable of the first pentagon and even in more cases of the rupture of those of the second pentagon (see Figures 7 and 8). Figure 8, shows that the absolute maximum displacement obtained for the loaded bridge was in case of the rupture of cable number 82 with a value equal to 6 cm.

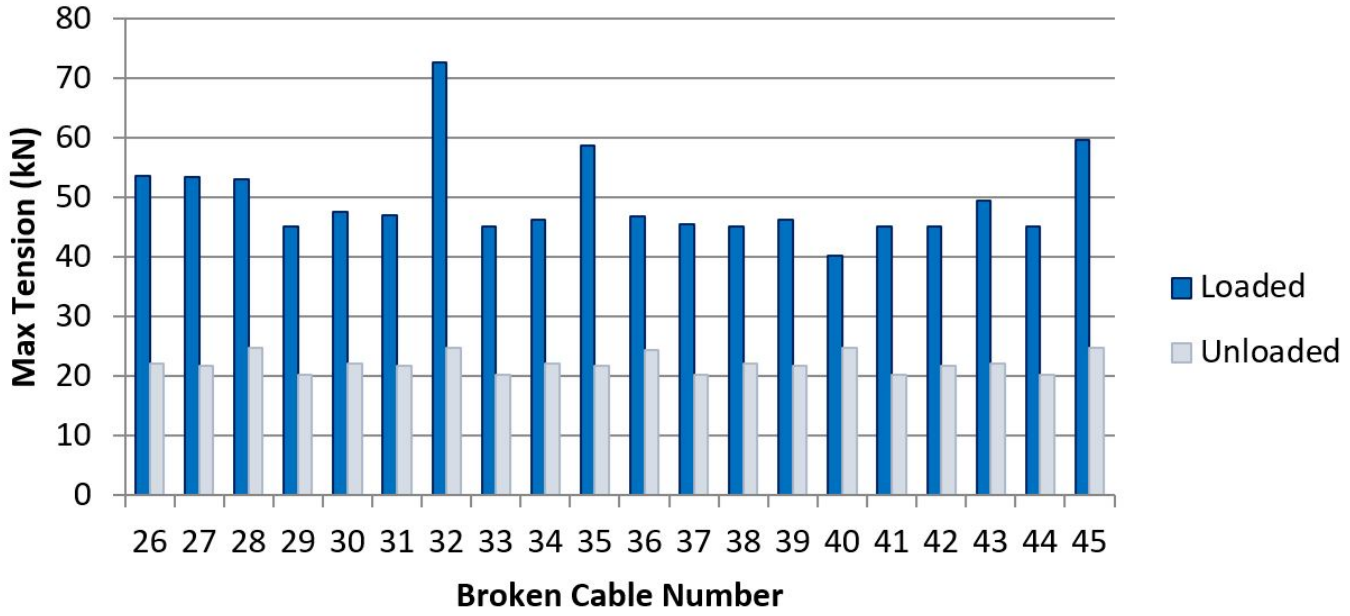


**Figure 3.** Maximum tension obtained for rupture of x-cables of the first pentagon

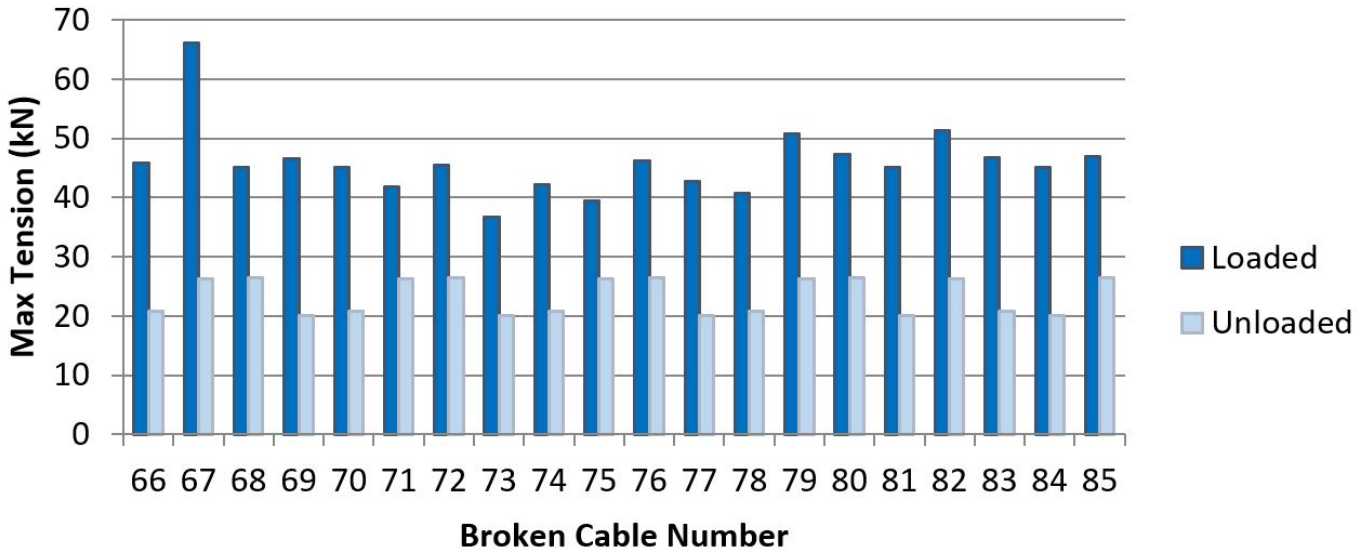


**Figure 4.** Maximum tension obtained for rupture of x-cables of the second pentagon

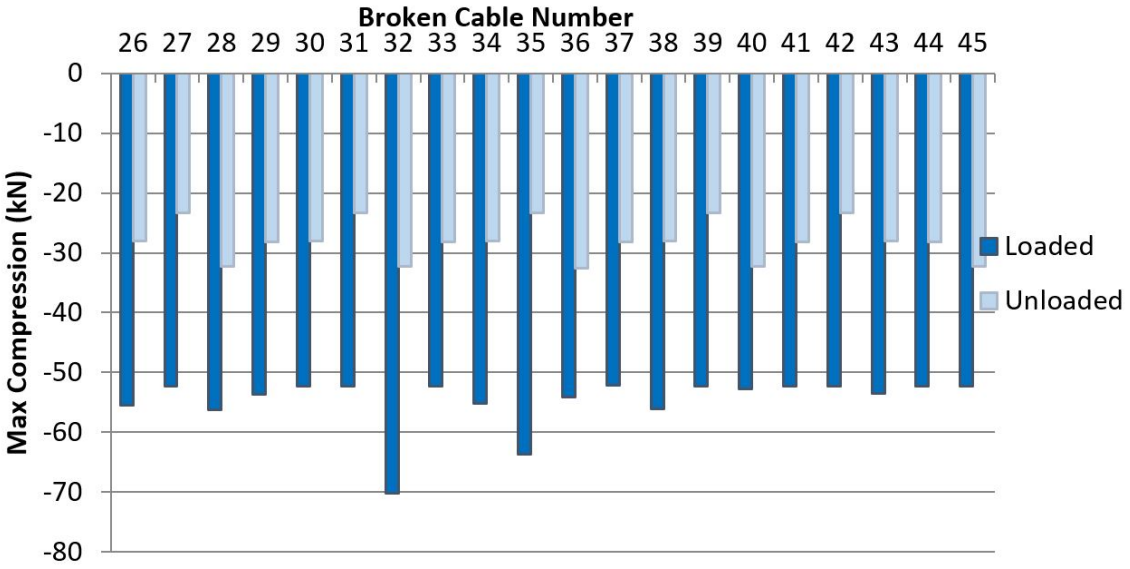


**Figure 5.** Maximum compression obtained for rupture of x-cables of the first pentagon

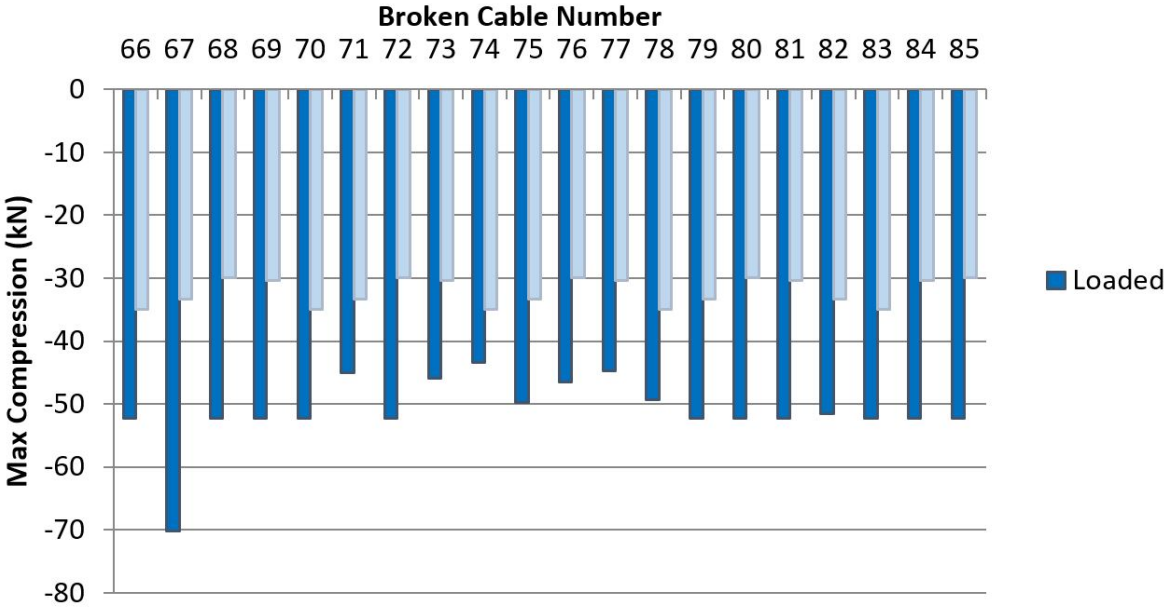


**Figure 6.** Maximum compression obtained for rupture of x-cables of the second pentagon

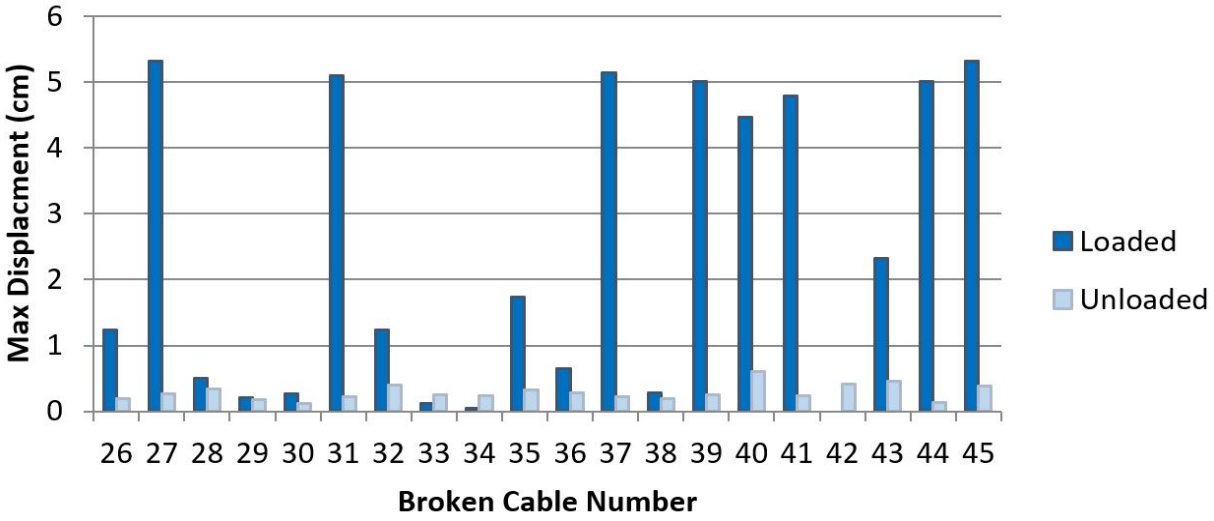


**Figure 7.** Maximum midspan average displacement obtained for rupture of x-cables of the first pentagon

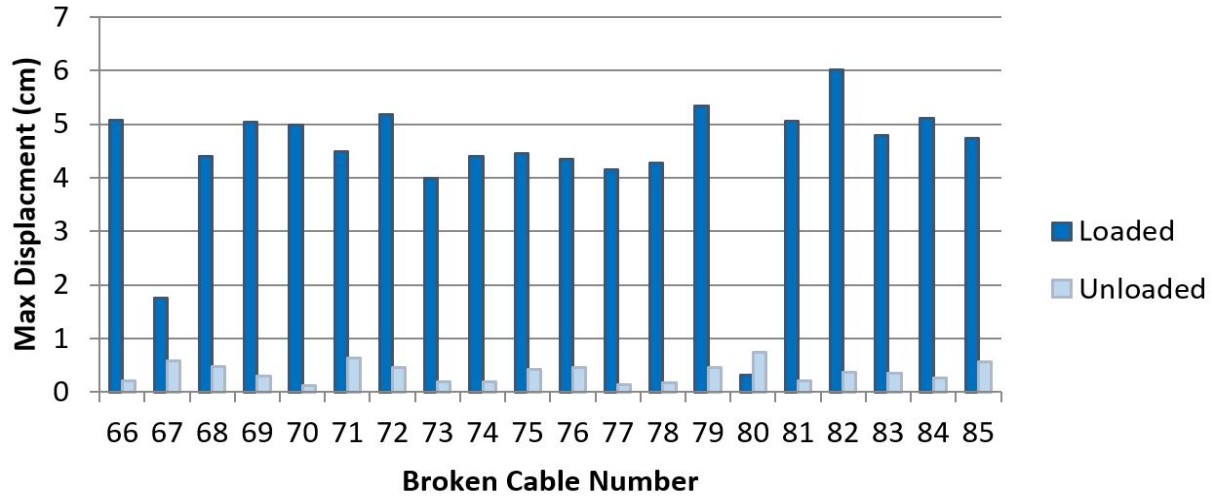


**Figure 8.** Maximum midspan average displacement obtained for rupture of x-cables of the second pentagon

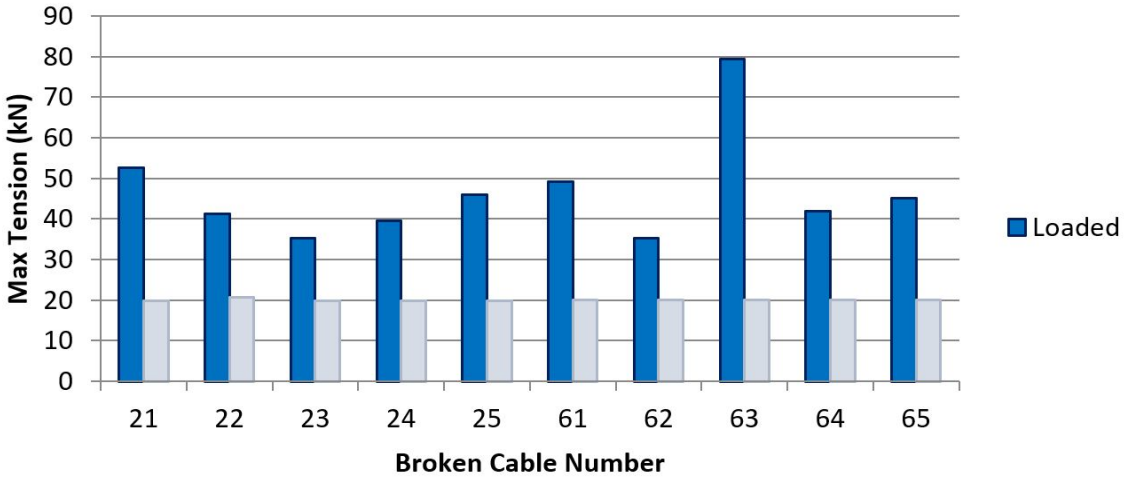


**Figure 9.** Maximum tension obtained for rupture of intermediate and middle pentagon layer cables

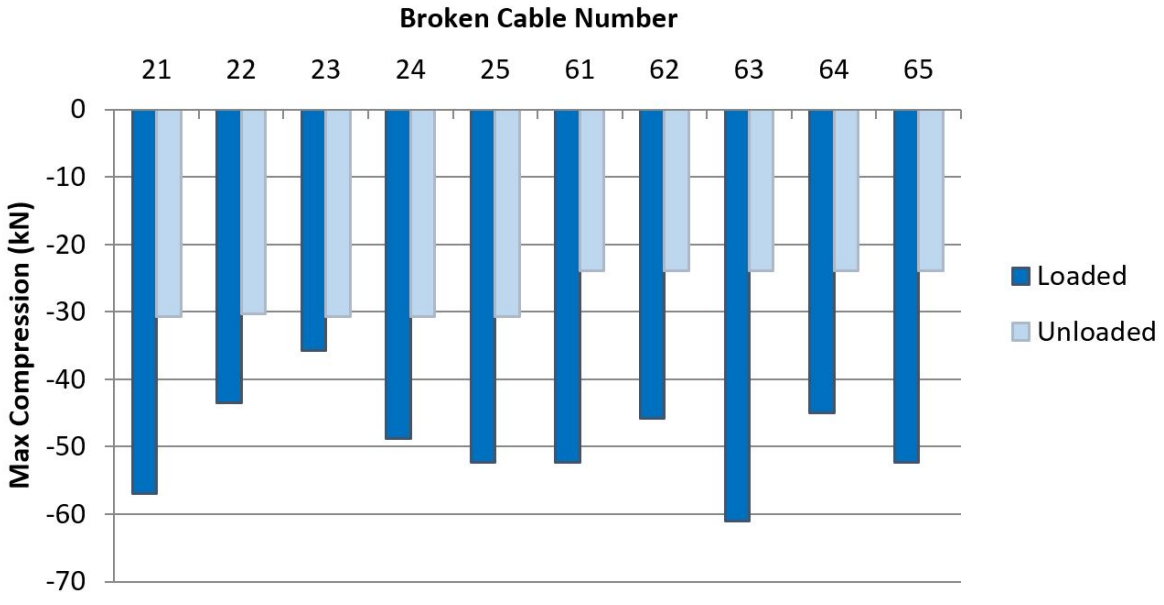


**Figure 10.** Maximum compression obtained for rupture of intermediate and middle pentagon layer cables

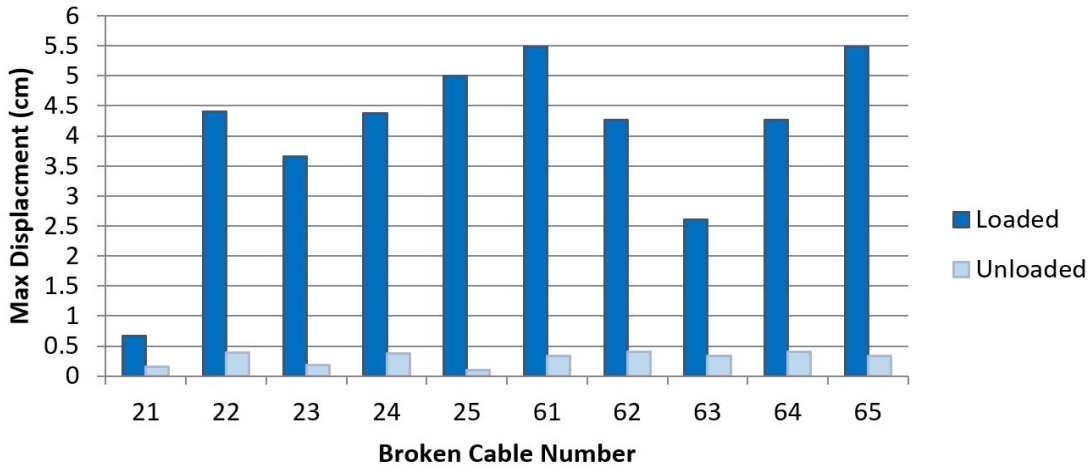


**Figure 11.** Maximum midspan average displacement obtained for rupture of intermediate and middle pentagon layer cables.

The results of the simulation of the rupture of the layer cables of the intermediate and middle pentagons are displayed in Figures 9 to 11. In case of the unloaded bridge, the maximum tension and compression, respectively in the bridge cables and struts were found to be way below their tension and compression capacities. However, in the case of the loaded structure, the values for the tensions and compressions became much larger and did not exceed their limit for almost all simulations. Only for the simulation of the rupture of the layer cable of the middle pentagon numbered 63, the tension capacity has been exceeded as shown in Figure 9. As for the middle node displacements, they all remained way below the limit for the unloaded bridge and exceeded the allowable values in most cases when the bridge was loaded (see Figure 11). In case of the rupture of the layer cables of the middle pentagon numbered 61 and 65, the maximum displacements reached 5.5 cm in both cases.

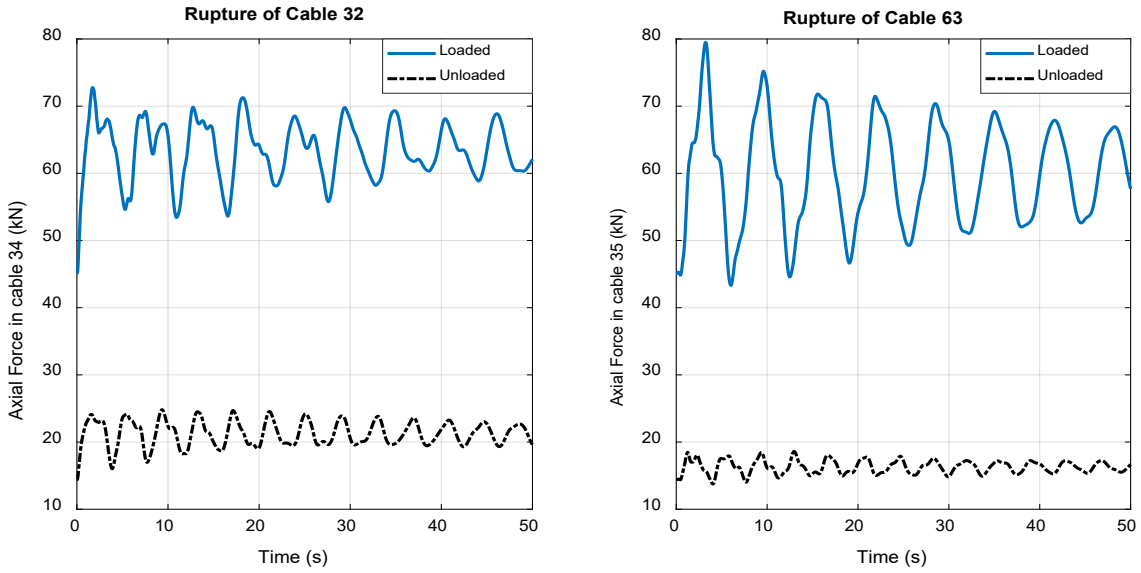


**Figure 12.** Evolution in time of tensions in cables 34 and 63, respectively for the rupture of cables 32 and 63.

Figure 12 shows the evolution in time of the tension forces in cables 34 and 63, respectively for the rupture of cables 32 and 63 in case of loaded and unloaded configurations of the tensegrity bridge. Large amplification factors of the tension in these two cables were obtained especially in case of the loaded bridge. For the same cases of rupture of cables 32 and 63, the time variations of the axial forces in struts 2 and 1 were plotted and are shown in Figure 13 for both the loaded and unloaded structure. Again, large variations of the compression forces were obtained in the loaded case but remained way below the strut's compression capacities.

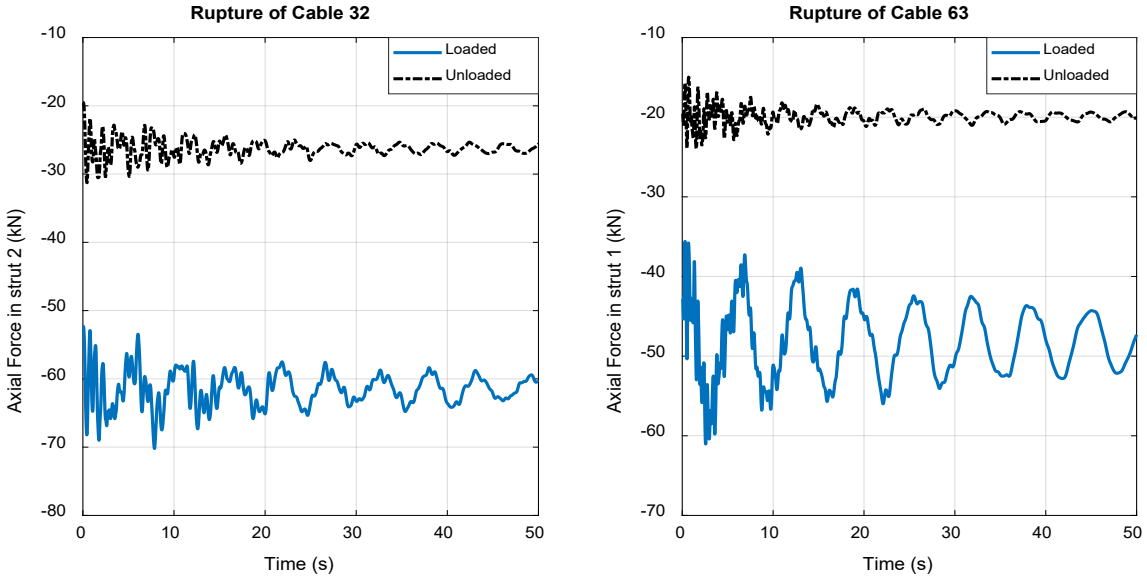


**Figure 13.** Evolution in time of axial forces in struts 2 and 1, respectively for the rupture of cables 32 and 63.

In order, to investigate the nonlinear dynamic instabilities of the tensegrity bridge, the time history evolution of the degree of stability, the relationship between the strain energy and its complementary part and the angle $\vartheta$ were determined for each simulation of cable rupture. For the rupture of cable 32 and 63, and for the case of the loaded structure, the evolution in time of the degree of stability has been plotted in Figure 14. This figure clearly shows that this factor fluctuates in the interval [-1, 1] which is an indication of the structure experiencing instant dynamic instabilities associated with the slackening of several cables. These dynamic instabilities are also highlighted in Figure 15, showing the variation of complementary strain energy as a function of strain energy when the rupture of cable 32 and 63 were simulated. Most of the data points obtained are not laying on the line $\Delta U^*=\Delta U$ but rather scattered around it and many are in quadrants n°2 and n°4. For the same cases, the angle between the axis $\Delta U$, and the line specified by the datum

(*ΔU*, ΔU*) and the origin of the axes and referred to as $\vartheta$, is plotted as a function of time and given in Figure 16. This figure shows that during the course of nonlinear dynamic response of bridge, many values of this angle were found to belong to the intervals [$\pi$/2, π] and [-$\pi$/2, 0], proving again that the structure undergoes instantaneous dynamic instabilities. The Time histories of the average midspan displacement of the loaded tensegrity bridge in case of the rupture of cable 82, exceeding the allowable deflection is given in Figure 17.

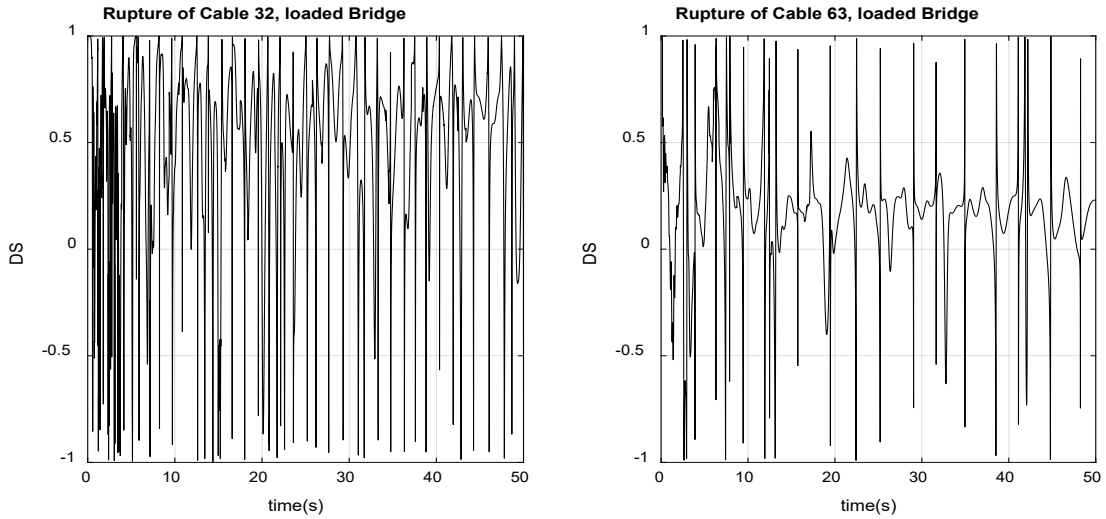


**Figure 14.** Time history evolution of the degree of stability respectively for the rupture of cables 32 and 63.

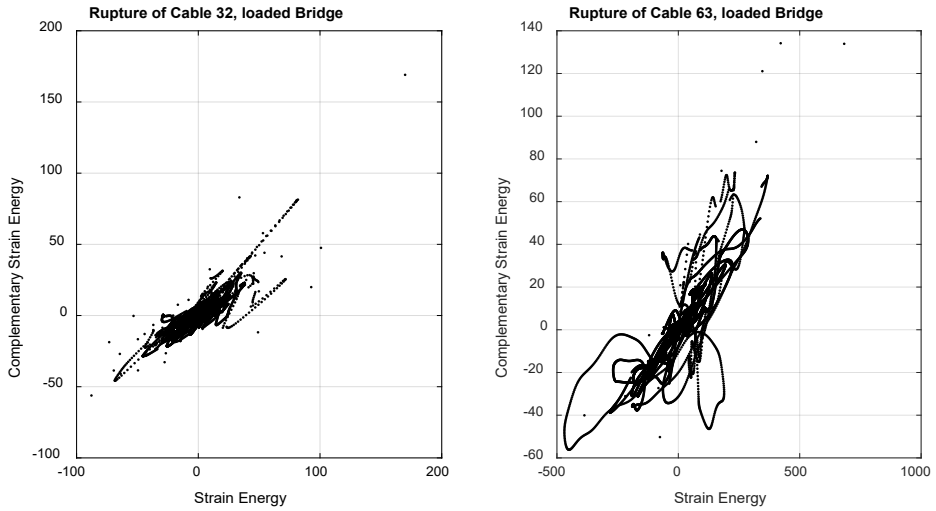


**Figure 15.** Relationship between the complementary strain energy and the strain energy respectively for the rupture of cables 32 and 63.

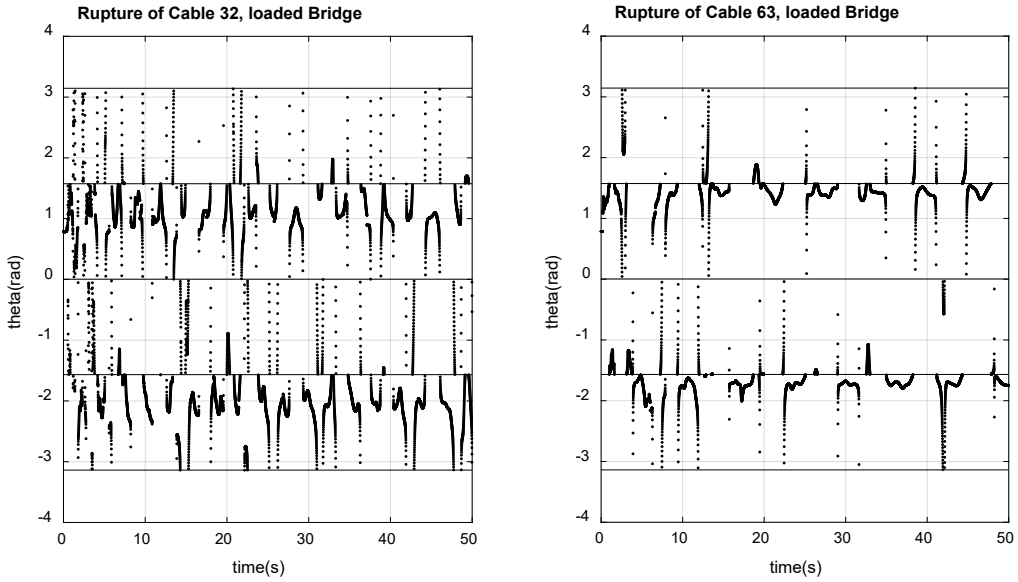


**Figure 16.** Time history evolution of the angle $\vartheta$respectively for the rupture of cables 32 and 63.

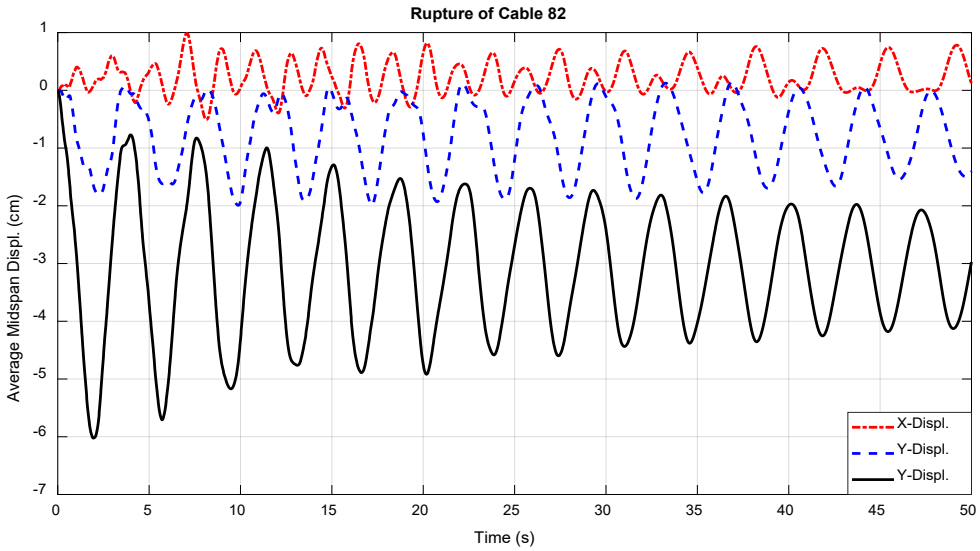


**Figure 17.** Time histories of the average midspan displacement of the loaded tensegrity bridge in case of the rupture of cable 82

## 8 CONCLUSIONS

The nonlinear dynamic response of a tensegrity bridge subjected to selected broken cables is investigated for two loading cases. The nonlinear equations of motion of the studied structure subjected to dynamic loading are numerically integrated using the unconditionally stable Newmark constant-average acceleration method combined with a Newton-Raphson iterative scheme. For all studied cable-rupture cases, the largest forces in cables and in struts as well as the largest average mid-span displacement are determined. For the unloaded bridge, the maximum tension values obtained in all cable elements were below their tension capacities whereas they exceeded them for only one case of the loaded case. However, the maximum compression forces obtained in the struts of the bridge were below their compression capacities for both loading cases. For several cases of cable rupture, the limit deflection at mid-span has been exceeded for the loaded bridge. Finally, nonlinear dynamic instabilities, caused by the slackening of cable, were observed in all simulations. It has been found that the tensegrity bridge undergoes instantaneous dynamic instabilities in several rupture cases.

## Acknowledgements

The authors gratefully acknowledge the project support (No. G.R.P.-125-39) provided by Deanship of Scientific Research, King Khalid University, Abha, Kingdom of Saudi Arabia, and also being thankful for providing the facilities required for the successful completion of the project.

**Author's Contributions:** Conceptualization, N Ben Kahla and N Belhadj Ali; Methodology, N Ben Kahla and MH El Ouni; Investigation, N Ben Kahla, MH EL Ouni and RA Khan; Writing - original draft, Ben Kahla, MH El Ouni, N Belhadj Ali and RA Khan and; Writing - review & editing, N Bel Hadj Ali and MH El Ouni; Funding acquisition, N Ben Kahla; Resources, N Ben Kahla; Supervision, N Ben Kahla and N Bel Hadj Ali.

**Editor:** Marco L. Bittencourt

## References

Al Sabouni-Zawadzka, A.; Gilewski, W. (2018) Inherent Properties of Smart Tensegrity Structures. Appl. Sci., 8, 787. https://doi.org/10.3390/app8050787

Atig, M., El Ouni, M. H. and Ben Kahla, N. (2019) “Dynamic stability analysis of tensegrity systems.” European Journal of Environmental and Civil Engineering, 23(6): 675-692.https://doi.org/10.1080/19648189.2017.1304275

Bel Hadj Ali, N. and Smith, I. F. C. (2010) “Dynamic behavior and vibration control of a tensegrity structure.” International Journal of Solids and Structures, 47(9): 1285-1296.DOI: 10.1016/j.ijsolstr.2010.01.012

Bel Hadj Ali, N., Rhode-Barbarigos, L., Pascual Albi, A. A. and Smith, I. F. C. (2010) “Design optimization and dynamic analysis of a tensegrity-based footbridge.” Engineering Structures, 32(11): 3650-3659.DOI: 10.1016/j.engstruct.2010.08.009

Ben Kahla, N. and Kebiche, K. (2000) “Nonlinear elastoplastic analysis of tensegrity systems.” Engineering Structures, 22(11): 1552-1566.https://doi.org/10.1016/S0141-0296(99)00088-7

Ben Kahla, N. and Moussa, B. (2002) “Effect of a Cable Rupture on Tensegrity Systems.” International Journal of Space Structures, 17(1): 51-65.https://doi.org/10.1260/026635102760123051

Blandford, G. E. (1996) “Large Deformation Analysis of Inelastic Space Truss Structures.” Journal of Structural Engineering, 122(4): 407-415.https://doi.org/10.1061/(ASCE)0733-9445(1996)122:4(407)

Connelly, R. and Terrell, M. (2005) “Globally rigid Symmetric Tensegrities.” Structural Topology 21.http://pi.math.cornell.edu/~connelly/Connelly.Terrell.pdf

El Ouni, M. H. and Ben Kahla, N. (2014) “Active tendon control of a Geiger dome.” Journal of Vibration and Control, 20(2): 241-255.https://doi.org/10.1177/1077546312458944

Faroughi, S. and Lee, J. (2014) “Geometrical Nonlinear Analysis of Tensegrity Based on a Co-Rotational Method.” Advances in Structural Engineering, 17(1): 41-51.DOI: 10.1016/j.ijmecsci.2015.01.015

González, A., Luoa, A., Shia D., (2019). Reconfiguration of multi-stage tensegrity structures using infinitesimal mechanisms. Latin American Journal of Solids and Structures, 16(3). http://dx.doi.org/10.1590/1679-78255331

He, Y. L., Chen, W. J., Dong, S. L. and Wang, Z. M. (2003) “The dynamic stability analysis of guyed masts under random wind loads.” Wind and Structures, 6(2): 151-164.https://doi.org/10.12989/was.2003.6.2.151

Kebiche, K., Kazi-Aoual, M. N. and Motro, R. (1999) “Geometrical non-linear analysis of tensegrity systems.” Engineering Structures, 21(9): 864-876.https://doi.org/10.1016/S0141-0296(98)00014-5

Lazopoulos, K. A. (2005). “Stability of an elastic tensegrity structure.” ActaMechanica, 179(1): 1-10.https://doi.org/10.1007/s00707-005-0244-0

Leu, L. J. and Yang, Y. B. (1990) “Effects of Rigid Body and Stretching on Nonlinear Analysis of Trusses.” Journal of Structural Engineering, 116(10): 2582-2598.https://doi.org/10.1061/(ASCE)0733-9445(1990)116:10(2582)

Michielsen, J., Fey, R. H. B. and Nijmeijer, H. (2012) “Steady-state dynamics of a 3D tensegrity structure: Simulations and experiments.” International Journal of Solids and Structures, 49(7): 973-988.DOI: https://doi.org/10.1016/j.ijsolstr.2011.12.011

Motro, R., Najari, S. and Jouanna, P. (1986) Static and Dynamic Analysis of Tensegrity Systems. ASCE International Symposium on Shells and Spatial Structures, Computational Aspects. Springer. New York, NY, USA, 270-279.DOI https://doi.org/10.1007/978-3-642-83015-0_24

Oh, C.L., Choong, K.K., Nishimura, T., Kim, J.Y., Hassanshahi, O. (2019). Shape change analysis of tensegrity models. Latin American Journal of Solids and Structures 16(7). https://doi.org/10.1590/1679-78255407

Ohsaki, M. and Zhang, J. (2006) “Stability conditions of prestressed pin-jointed structures.” International Journal of Non-Linear Mechanics, 41(10): 1109-1117.https://doi.org/10.1016/j.ijnonlinmec.2006.10.009

Oppenheim, I. J. and Williams, W. O. (2001) “Vibration and Damping in Three-Bar Tensegrity Structure.” Journal of Aerospace Engineering, 14(3): 85-91. https://doi.org/10.1061/(ASCE)0893-1321(2001)14:3(85)

Skelton, R. E. and de Oliveira, M. C. Tensegrity systems, Springer 2009.https://doi.org/10.1007/978-0-387-74242-7

Sultan, C., Corless, M. and Skelton, R. E. (2002) “Linear dynamics of tensegrity structures.” Engineering Structures, 24(6): 671-685.DOI: 10.1016/S0141-0296(01)00130-4

Sychterz, A. C. and Smith, I. F. C. (2018) “Using dynamic measurements to detect and locate ruptured cables on a tensegrity structure.” Engineering Structures, 173: 631-642.DOI: 10.1016/j.engstruct.2018.06.083

Tan, G. E. B. and Pellegrino, S. (2008) “Nonlinear vibration of cable-stiffened pantographic deployable structures.” Journal of Sound and Vibration, 314(3): 783-802.https://doi.org/10.1016/j.jsv.2008.01.022

Tran, H. C. and Lee, J. (2011) “Geometric and material nonlinear analysis of tensegrity structures.” ActaMechanicaSinica, 27(6): 938-949.https://link.springer.com/article/10.1007/s10409-011-0520-2

Xiao, N., Miao, Y. Z. and Chen, H. P. (2011) Active vibration control of cable-strut tensegrity structures under wind. 5th Cross-strait Conference on Structural and Geotechnical Engineering, Hong Kong, China